

Parametric Spatio-Temporal Control of Focusing Laser Pulses

Matthew A. Coughlan, Mateusz Plewicki, and Robert J. Levis*

Department of Chemistry, Center for Advanced Photonics Research, Temple University, Philadelphia, Pennsylvania 19122, USA

*rjlevis@temple.edu

Abstract: Simultaneous spatial and temporal focusing pulses are created using parametric pulse shaping and characterized with scanning SEA TADPOLE. Multiple foci are created with optically-controlled longitudinal and transverse spatial positions. The characterized foci are in agreement with the predictions of a Fourier optics model. The measurements reveal significant pulse front tilt resulting from the simultaneous spatial and temporal focusing optics.

©2009 Optical Society of America

OCIS codes: (140.3300) Laser beam shaping; (140.3510) Laser Fiber

References and links

1. J. Bewersdorf, R. Pick, and S. W. Hell, "Multifocal multiphoton microscopy," *Opt. Lett.* **23**(9), 655–657 (1998).
2. R. Carriles, K. E. Sheetz, E. E. Hoover, J. A. Squier, and V. Barzda, "Simultaneous multifocal, multiphoton, photon counting microscopy," *Opt. Express* **16**(14), 10364–10371 (2008).
3. E. Chandler, E. Hoover, J. Field, K. Sheetz, W. Amir, R. Carriles, S. Y. Ding, and J. Squier, "High-resolution mosaic imaging with multifocal, multiphoton photon-counting microscopy," *Appl. Opt.* **48**(11), 2067–2077 (2009).
4. D. Oron, E. Tal, and Y. Silberberg, "Scanningless depth-resolved microscopy," *Opt. Express* **13**(5), 1468–1476 (2005).
5. E. Papagiakoumou, V. de Sars, D. Oron, and V. Emiliani, "Patterned two-photon illumination by spatiotemporal shaping of ultrashort pulses," *Opt. Express* **16**(26), 22039–22047 (2008).
6. G. Duemani Reddy, K. Kelleher, R. Fink, and P. Saggau, "Three-dimensional random access multiphoton microscopy for functional imaging of neuronal activity," *Nat. Neurosci.* **11**(6), 713–720 (2008).
7. K. E. Sheetz, E. E. Hoover, R. Carriles, D. Kleinfeld, and J. A. Squier, "Advancing multifocal nonlinear microscopy: development and application of a novel multibeam Yb:KGd(WO₄)₂ oscillator," *Opt. Express* **16**(22), 17574–17584 (2008).
8. T. Feurer, J. C. Vaughan, R. M. Koehl, and K. A. Nelson, "Multidimensional control of femtosecond pulses by use of a programmable liquid-crystal matrix," *Opt. Lett.* **27**(8), 652–654 (2002).
9. T. Feurer, J. C. Vaughan, and K. A. Nelson, "Spatiotemporal coherent control of lattice vibrational waves," *Science* **299**(5605), 374–377 (2003).
10. M. E. Durst, G. Zhu, and C. Xu, "Simultaneous spatial and temporal focusing for axial scanning," *Opt. Express* **14**(25), 12243–12254 (2006).
11. M. E. Durst, G. Zhu, and C. Xu, "Simultaneous spatial and temporal focusing in nonlinear microscopy," *Opt. Commun.* **281**(7), 1796–1805 (2008).
12. G. Zhu, J. van Howe, M. Durst, W. Zipfel, and C. Xu, "Simultaneous spatial and temporal focusing of femtosecond pulses," *Opt. Express* **13**(6), 2153–2159 (2005).
13. H. Suchowski, D. Oron, and Y. Silberberg, "Generation of a dark nonlinear focus by spatio-temporal coherent control," *Opt. Commun.* **264**(2), 482–487 (2006).
14. H. Suchowski, A. Natan, B. D. Bruner, and Y. Silberberg, "Spatio-temporal coherent control of atomic systems: weak to strong field transition and breaking of symmetry in 2D maps," *J. Phys. At. Mol. Opt. Phys.* **41**(7), 074008 (2008).
15. E. Papagiakoumou, V. de Sars, V. Emiliani, and D. Oron, "Temporal focusing with spatially modulated excitation," *Opt. Express* **17**(7), 5391–5401 (2009).
16. P. Bowlan, U. Fuchs, R. Trebino, and U. D. Zeitner, "Measuring the spatiotemporal electric field of tightly focused ultrashort pulses with sub-micron spatial resolution," *Opt. Express* **16**(18), 13663–13675 (2008).
17. P. Bowlan, P. Gabolde, M. A. Coughlan, R. Trebino, and R. J. Levis, "Measuring the spatiotemporal electric field of ultrashort pulses with high spatial and spectral resolution," *J. Opt. Soc. Am. B* **25**(6), A81–A92 (2008).
18. P. Bowlan, P. Gabolde, and R. Trebino, "Directly measuring the spatio-temporal electric field of focusing ultrashort pulses," *Opt. Express* **15**(16), 10219–10230 (2007).

19. A. M. Weiner, "Femtosecond pulse shaping using spatial light modulators," *Rev. Sci. Instrum.* **71**(5), 1929–1960 (2000).
20. M. A. Coughlan, M. Plewicky, S. M. Weber, P. Bowlan, R. Trebino, and R. J. Levis, "Shaped pulse electric-field construction and interferometric characterization: The SPECIFIC method," *N. J. Phys.* Submitted.
21. M. A. Coughlan, M. Plewicky, S. M. Weber, P. Bowlan, R. Trebino, and R. J. Levis, "Shaped pulse electric-field construction and interferometric characterization: The SPECIFIC method," arXiv:0903.1233v1 (2009).
22. S. M. Weber, "New concepts for optimal control experiments using femtosecond pulse shaping," in *Physics* (Free University, Berlin, 2007).
23. S. M. Weber, A. Lindinger, F. Vetter, M. Plewicky, A. Merli, and L. Wöste, "Application of parametric time and frequency domain shaping," *Eur. Phys. J. D* **33**, 39–42 (2005).
24. S. M. Weber, F. Weise, M. Plewicky, and A. Lindinger, "Interferometric generation of parametrically shaped polarization pulses," *Appl. Opt.* **46**(23), 5987–5990 (2007).
25. S. Akturk, X. Gu, E. Zeek, and R. Trebino, "Pulse-front tilt caused by spatial and temporal chirp," *Opt. Express* **12**(19), 4399–4410 (2004).
26. Z. Bor, B. Racz, G. Szabo, M. Hilbert, and H. A. Hazim, "Femtosecond pulse front tilt caused by angular dispersion," *Opt. Eng.* **32**(10), 2501–2504 (1993).
27. J. Hebling, "Derivation of the pulse front tilt caused by angular dispersion," *Opt. Quantum Electron.* **28**(12), 1759–1763 (1996).
28. J. W. Goodman, *Introduction to Fourier optics* (Roberts & Co, 2005).
29. M. M. Wefers, and K. A. Nelson, "Space-time profiles of shaped ultrafast optical waveforms," *IEEE J. Quantum Electron.* **32**(1), 161–172 (1996).
30. W. Amir, R. Carriles, E. E. Hoover, T. A. Planchon, C. G. Durfee, and J. A. Squier, "Simultaneous imaging of multiple focal planes using a two-photon scanning microscope," *Opt. Lett.* **32**(12), 1731–1733 (2007).

1. Introduction

Acquiring a high resolution image in the shortest amount of time is desirable for many applications including whole cell analysis, materials characterization, optical sectioning, and tomography. In addition to increasing the raster scan rate and signal to noise level, this can be accomplished by multiplexing multiple foci [1–7]. The latter represents a challenging task and is an active area of current research. For example, multiple transverse foci can be generated using a microarray lens [1] or by generating multiple beam positions on an output coupler in a Ti:Sapphire oscillator cavity [7]. Two longitudinal foci have been generated using a Michelson interferometer with one arm containing a deformable mirror to modify the beam divergence [2]. After recombination and passage through a microscope objective, two different focal lengths are produced. We report here a new method to produce multiple longitudinal and transverse foci with tunable separation by combining laser pulse shaping with spatial temporal focusing.

Spatio-temporal pulse shaping was first demonstrated with real space and wavevector shaping in a BBO crystal [8]. An input pulse was modulated using a two-dimensional liquid crystal array to produce an electric field with a spatially variable spectral phase [8, 9]. Spatio-temporal focusing of a femtosecond laser pulses was then developed in two groups to provide scanningless depth-resolved images of biological and material samples by imaging two-photon laser induced fluorescence with a CCD camera [4, 10]. Spatio-temporal focusing or simultaneous spatial and temporal focusing (SSTF) occurs when the bandwidth of a spatially chirped beam is combined through the process of focusing to create a transform-limited pulse at the focal position as shown in Fig. 1. The optics required to create spatio-temporal focusing consist of a diffraction grating, a collimating lens, and a focusing lens, see Fig. 2. The combination of a diffraction grating and collimating lens serves to

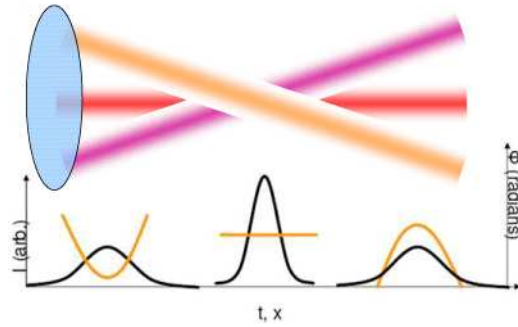


Fig. 1. Relation between position in the spatial focus and pulse duration. The three colors represent different spectral components of a spatially and temporally chirped beam.

spatially separate the frequency components (in a spectrometer configuration). This necessarily increases the pulse duration for any given spatial area of the beam. The spatially and temporally chirped pulse is then focused by an objective lens, and as the pulse propagates to the focus the spatial and temporal chirp is subtracted at a rate proportional to the curvature of the objective lens. The temporal focus forms at the spatial focus (assuming a transform-limited input pulse) when the spatially separated frequency components are recombined at the focus of the objective lens. This increases the bandwidth of the pulse, resulting in temporal compression.

With SSTF, two photon excitation is highly dependent on the longitudinal position in the focusing beam, essentially occurring at the focal plane. This is due to the temporal compression occurring as the pulse approaches the spatial focus, with subsequent stretching after the focus. This effect was confirmed by measuring the cross-correlation through the SSTF focus [11, 12]. A 4-f pulse shaper was then used to longitudinally translate the spatial position of the temporal focus [13]. Longitudinal spatial control of a dark temporal focus was demonstrated by adding together second order spectral phase with a π step (centered on the fundamental two-photon absorption frequency). Simultaneous spatial and temporal focusing pulses have also been used to spatially discriminate weak and strong field quantum processes [14]. In such experiments it was shown that as the intensity of the pulse is increased, effects such as power broadening and Stark shifting break the spatial symmetry of the two-photon laser induced fluorescence in atomic cesium and rubidium. These experiments demonstrate that SSTF is much more versatile and can be used for other applications besides imaging.

The excitation of multiple imaging regions has been reported, using wavefront beam shaping of a femtosecond laser pulse with a liquid crystal spatial light modulator followed by a spatio-temporal focusing [5, 15]. Spatially shaping the input beam creates an intensity pattern that is imaged at the focal plane of an objective lens. By positioning a sample of interest in this region, multiple sections of excitation for multiphoton imaging can be produced. Combining spatial shaping and temporal focusing generates depth-resolved images of samples of interest.

In this work, we report that pulse shaping with carefully programmed waveforms in the temporal domain can be directly mapped to spatial position within the focus of an imaging system. Second order spectral phases can move the position of single foci in the SSTF imaging setup. Moreover, we report that this concept can be scaled up to a train of pulses with varying amounts of second order phase and relative delays predetermined by the user. We show that each pulse in the pulse train can have differing amounts of second order phase which permits the user to specify where that pulse is to compress within the focus of the objective lens. These conditions generate multiple longitudinal foci in the focus of the objective lens. We demonstrate that the linear phase, determining the pulses temporal delay,

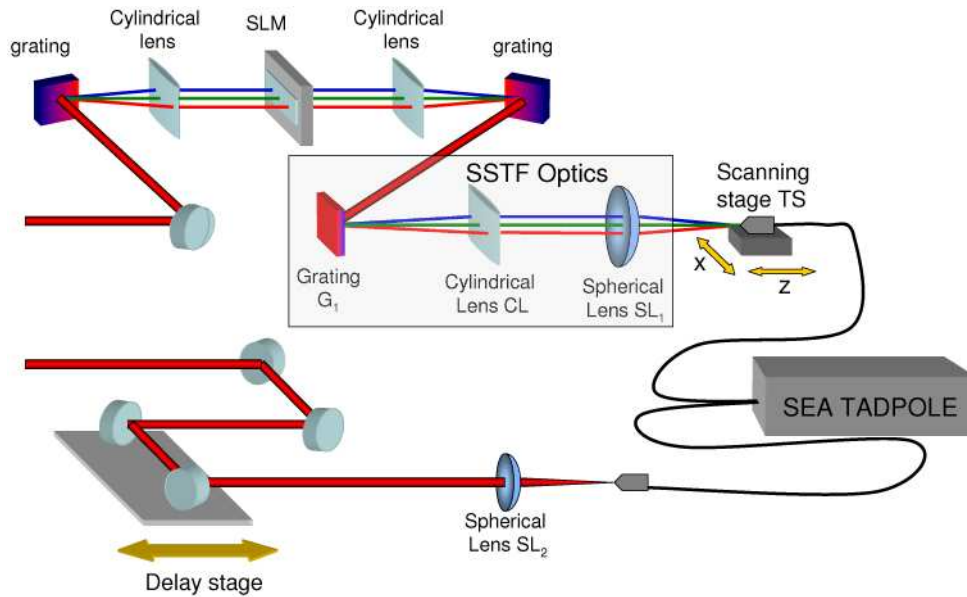


Fig. 2. Experimental multifoci setup with elements described as follows: G_1 1200 grooves/mm diffraction grating, CL Cylindrical Lens ($f=15\text{cm}$), SL_1 Spherical Lens ($f=5\text{cm}$), SL_2 Spherical Lens ($f=10\text{cm}$), TS X/Z scanning translation stage. Single mode optical fibers (core diameter = $5.6\mu\text{m}$) are used in SEA TADPOLE and a linear translation stage is adjusted the proper temporal overlap between reference and shaped pulses.

also separates the pulses laterally in the focus of the objective lens. Therefore the amount of linear phase of a pulse is directly mapped to transverse position of the focusing pulses of the objective lens. We confirm theoretically that linear phase ramps applied by the pulse shaper translate the focal spot laterally in the focus of the objective lens. The driving pulses are designed using a parametric pulse-shaping algorithm combined with the standard 1 dimensional 256-element pixilated liquid crystal modulator. The evolution of the spatio-temporal intensities along the focusing beam path are characterized using scanning SEA TADPOLE measurements [16–18]. This characterization reveals several new features including pulse front tilt and the ability to control both longitudinal and lateral focal spot position. This feature opens the possibility for multiplexed multiphoton microscopy studies and scanning a sample in two dimensions without any moving parts.

2. Experimental setup

The optical system for generating and characterizing multiple temporal foci is illustrated in Fig. 2. The laser source was an 86MHz Ti:Sapphire femtosecond oscillator producing pulses with approximately 20nm FWHM of bandwidth centered at 800nm and $\sim 5\text{nJ}$ energy per pulse. The laser beam is first collimated by a telescope to $\sim 2\text{mm}$ $1/e$ spot size. Next, a small portion of the beam is split off as a reference beam for the SEA TADPOLE detection, whereas the main part is directed to the pulse shaper. The shaper is an all reflective folded design (symbolically depicted in Fig. 2 as standard transmissive 4-f setup) including 1200 l/mm gold coated grating followed by 200 mm focusing element and CRI (Cambridge Research Instruments) SLM-2 X 128 modulator in the Fourier plane. The modulator is a 128 pixel device with phase and amplitude shaping capability, $97\mu\text{m}$ pixel size, and $3\mu\text{m}$ interpixel gap. Given the $\sim 2\text{mm}$ spot size on the grating the single frequency component focal spot size at the Fourier plane is on the order of $\sim 100\mu\text{m}$ which is the size of a single pixel. Theory [19] predicts that pixilation effects and side pulses should be diminished for our optical setup. Replica pulses are present in our experiments, as they are difficult to completely remove, and have an intensity of $<10\%$ of the main temporal features maximum intensity.

The SSTF apparatus consists of a 1200 l/mm grating followed by a 15cm focal length cylindrical lens and 5cm focal length spherical lens. In the present experiment the pulse shaping and spatio-temporal focusing are separated for two reasons. The shaper is well-calibrated for obtaining the required high quality pulse shapes. Separation of shaping stage from spatio-temporal focusing also allows for manipulation of the frequency spread in the SSTF Fourier plane by changing either the cylindrical lens or SSTF grating.

Parametric pulse shaping is used to calculate a user-specified pulse shape in the spectral domain, for application to the spatial light modulator [20–24]. SEA TADPOLE is employed to characterize the parametric pulse shapes. The SEA TADPOLE system was operated in scanning mode with the input fiber tip placed on a computer-controlled stage scanning in a direction transverse to the laser pulse propagation direction. For each longitudinal position of the scanning fiber tip, zero delay was reset with the reference pulse. The temporal field was recorded at each transverse position and compiled to generate a plot of temporal delay versus transverse position. This procedure was performed for each longitudinal position in the objective lens focal volume.

3. Data and Analysis

The lateral and longitudinal electric field characterization of the spatially and temporally focusing pulse is displayed in Fig. 3 for the case of flat phase and amplitude on the pulse shaper. The visualization of the following SSTF experiments is presented in series of five panels for longitudinal positions (z coordinate) of -1mm , -0.5mm , 0mm , 0.5mm , and 1mm with respect to the focus. The negative values correspond to longitudinal positions that occur before the focus. Each panel is a 2-dimensional representation of the temporal evolution of the electric field as a function of transverse position across the beam (x coordinate). At the longitudinal position 1 mm before the optical focus, panel a, the pulse duration is approximately 1 ps and has considerable pulse front tilt. The pulse front tilt is illustrated by the fact that the left side ($x = -0.2\text{mm}$) of the pulse arrives at the -1mm plane approximately 5ps before the right side ($x = 0.2\text{mm}$). A pulse front with no tilt would be represented by a vertical intensity distribution at time zero with the thickness of the line representing the pulse duration. At -0.5mm before the temporal focus, panel b, the pulse duration is 500fs with no apparent change in pulse front tilt. At the approximate temporal focus, panel c, the pulse duration converges to 100fs and the pulse front tilt remains. Beyond the temporal focus, the pulse duration increases again as seen in panels d and e.

Pulse front tilt is defined as the difference in the arrival time to a spatial plane orthogonal to the propagation direction. In the apparatus employed here, the angular dispersion introduced by the diffraction grating together with the finite incident beam diameter results in differing path lengths in the transverse direction. The telescope in the SSTF optics later magnifies the pulse front tilt. The magnitude of the pulse front tilt is a function of the incidence angle and the spot size on the grating, grating density and the telescope parameters [25–27]. The spatio-temporal measurements in Fig. 3 provide a clear indication that there is a linear relationship between the pulse arrival as a function of transverse position in the beam.

The measurements in Fig. 3 reveal that the temporal width decreases as the pulse propagates to the temporal focus and then increases thereafter. This process is a consequence of the spatially dependent spectral overlap of each dispersed frequency component depicted in Fig. 1, and the spectral phase evolution along the beam propagation axis. The later is due to coupling of the spectral phase with the wavefront at the Fourier plane of the SSTF setup. The objective lens modifies the pulse wavefront, creating a parabolic curvature, which

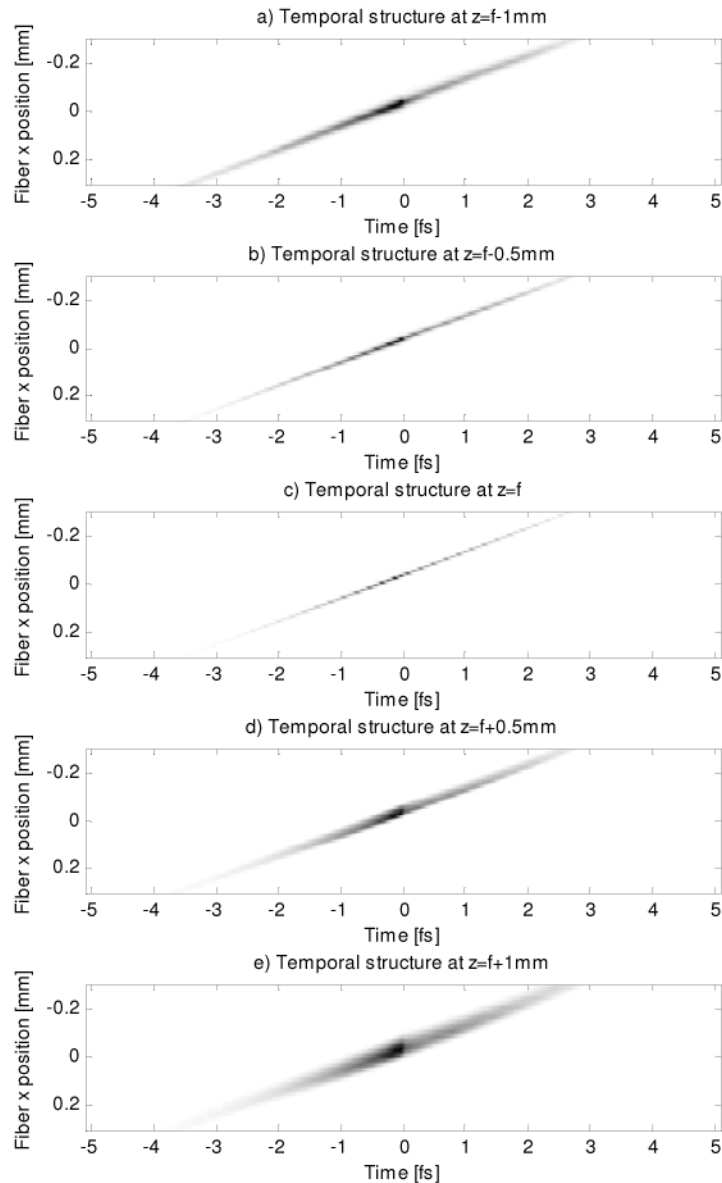


Fig. 3. Measurement of S.S.T.F. without pulse shaping. a) $z=f-1\text{mm}$ b) $z=f-0.5\text{mm}$ c) $z=f$ d) $z=f+0.5\text{mm}$ e) $z=f+1\text{mm}$, where f is a focal length.

subsequently yields an overall quadratic spectral phase and lengthens the pulse duration. During the propagation to the focal plane, the wavefront curvature approaches zero, resulting in maximal compression of the pulse. After the temporal focus the process is reversed, the second order phase changes sign and the duration of the pulse increases again (inset in Fig. 1).

Using the parametric shaping algorithm, two pulses can be produced with a well-defined temporal delay. Two temporally separated pulses traversing through the SSTF optics and focusing through the objective lens would result in two pulses that temporally compress and stretch equally through all spatial coordinates. With parametric shaping the pulses

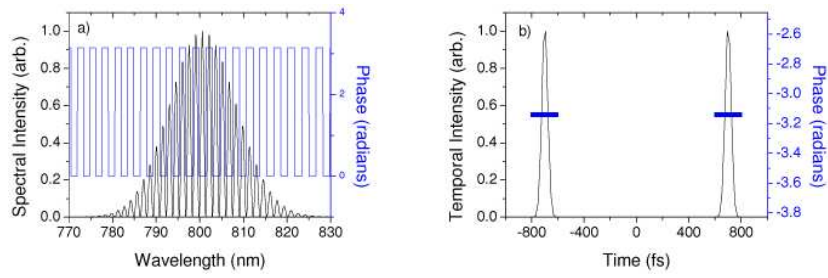


Fig. 4. Spectral and temporal profile designed and applied by the shaping algorithm. Two pulse separated by 1400fs with flat phases.

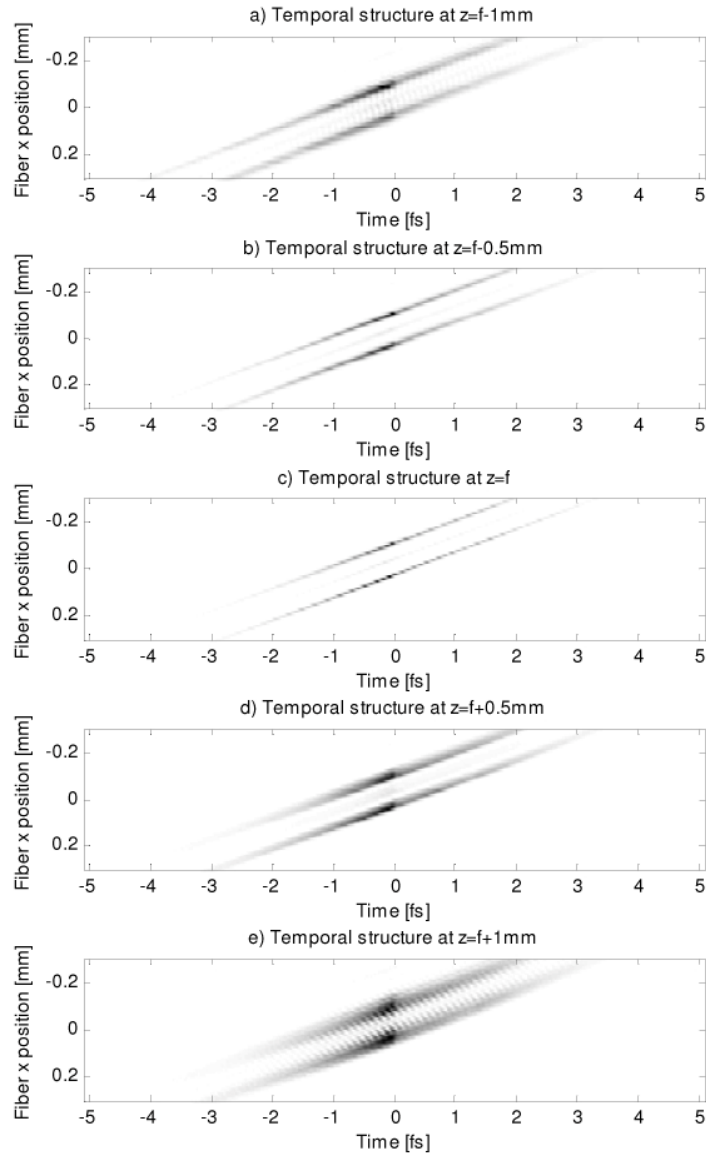


Fig. 5. Measured evolution of the temporal intensity of the two pulse structure from Fig. 4. shaping. a) $z=f-1\text{mm}$ b) $z=f-0.5\text{mm}$ c) $z=f$ d) $z=f+0.5\text{mm}$ e) $z=f+1\text{mm}$, where f is a focal length.

can be temporally and spatially decoupled at the temporal focus. Scanning SEA TADPOLE measurements can be used to reveal the spatio-temporal electric field evolution of the SSTF pulse. The calculated spectral and temporal phase and amplitude mask for the multiple foci pulse is shown in Fig. 4. Figure 4a shows the characteristic π step spectral phase pattern resulting from the superposition of two phase ramps. The spectral intensity profile is the interference pattern of two pulses. The temporal intensity profile shown in Fig. 4 b consists of two sub-pulses with an interpulse delay of 1.4 ps, with flat temporal phase for both pulses. The SEA TADPOLE measurements of the evolution of the spatio-temporal electric field for this pulse shape in the vicinity of the focus are shown in Fig. 5. Figure 5a clearly shows that there are two pulse fronts as expected from the predicted parametric pulse shapes displayed in Fig. 4. The 1.4 ps delay between the two pulses is also manifested in the separation of the pulses along the x-axis transverse to the propagation direction. The physical separation of the pulse fronts is a result of the linear spectral phase term applied to each sub pulse. The linear spectral phase, defining the temporal delay between the two pulses adds to the parabolic phase from the spherical lens. The result is a shift in the focus of the delayed pulse along the x-axis for each plot in Fig. 5. This would be equivalent to translating the lens in the x direction in Fig. 1. One conclusion from this experiment is that spectral phase manipulation will allow for both depth and lateral scanning of the sample with no moving parts. In addition, when using the pulse shaper, pulse structures can be generated with individual and independent phase characteristics for each sub pulse resulting in the ability to manipulate each sub pulse's spatio-temporal position independently. Figure 5 demonstrates the ability to focus two pulses to the same longitudinal position.

The effects of the spectral phase and amplitude masks on the spatio-temporal electric field propagating to the temporal focus can be understood using Fourier optics [28]. We build on the mathematical description of the SSTF pulse propagation as set forth previously [10–12]. The laser field at the Fourier plane of the objective lens can be represented by:

$$A_0(x, \Delta\omega) = A_0 \exp\left(-\frac{\Delta\omega^2}{\Omega^2}\right) \exp\left(-\frac{(x - \alpha\Delta\omega)^2}{s^2}\right) \exp\left(-i(\delta\Delta\omega + \beta\Delta\omega^2)\right), \quad (1)$$

where A_0 is a normalization constant, $\Delta\omega = \omega - \omega_0$ is the relative frequency, $\Omega (2\ln 2)^{1/2}$ is the FWHM of the bandwidth of the pulse, $s(2\ln 2)^{1/2}$ is a transverse beam FWHM for a given frequency $\Delta\omega$, $\alpha\Delta\omega$ describes the shift from the optical axis of the lens of the frequency component $\Delta\omega$, δ describes the linear phase and β describes the second order phase. The linear phase term has not been considered in previous Fourier description of the SSTF field. Propagation of the pulse and Fourier transforming the result to the temporal domain leads to a description of the intensity of the field in the form of $I(x, z, (t - \delta))$ as a function of spatial coordinates x , z , and time. It is important to note that the linear phase term δ is only coupled to time and there are no mixed terms of linear phase with transverse position, thus the linear phase influence is limited to shifting the pulse in time.

The function for $I(x, z, (t - \delta))$ correctly describes spatio-temporal position for the longitudinal focus via dispersion control through the quadratic phase parameter β [12]. However, this expression implies that the transverse spatial coordinate cannot be changed because δ is not coupled to the x (transverse) dimension. To illustrate the longitudinal and transverse position of maximum spatial intensity distribution we consider the case of two-photon excitation (TPE). The TPE probability is given by:

$$TPE(x, z) = \int_{-\infty}^{+\infty} (I(x, z, (t - \delta)))^2 dt \quad (2)$$

Due to coupling of the linear phase term only with temporal coordinate, the TPE spatial distribution will not change as a function of delta. This implies that the assumptions used in

previous treatments [10–12] for SSTF used in Eq. (1) are insufficient to model transverse motion

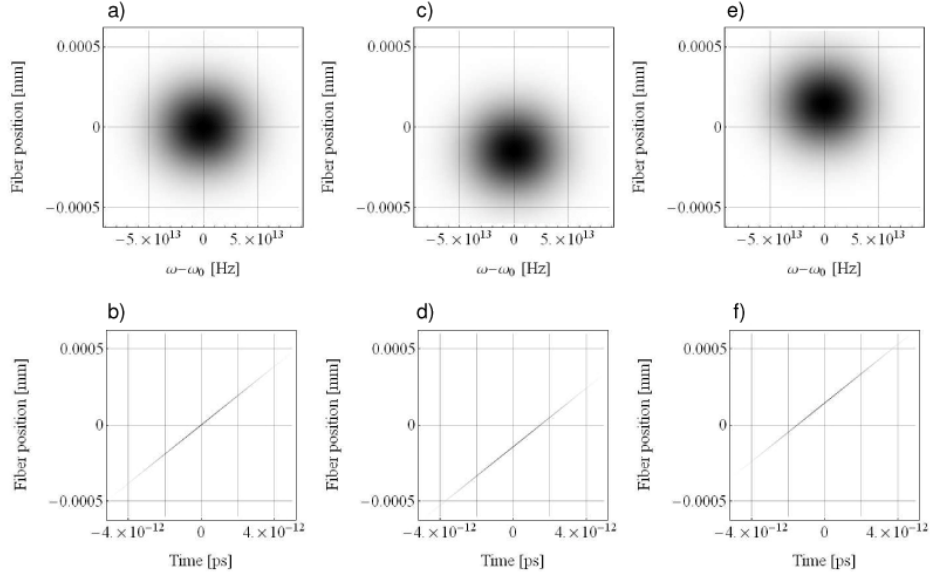


Fig. 6. Simulation of spatio-spectral distribution (top row) and spatio-temporal pulse structure (bottom row) at the wave front modulation on beam corresponding to (a and b) no phase ramp, (c and d) phase ramp corresponding to delay 1.5ps (c and d), and -1.5ps (e and f).

of the focus with linear phase ramp, as seen in Fig. 6. The coupling between δ and x can be modeled mathematically using wavefront modulation ($\varphi(x)=\delta_x x + \beta_x x^2$) in the Fourier plane of the SSTF setup instead of spectral phase modulation ($\varphi(\omega)=\delta_\omega \Delta\omega + \beta_\omega \Delta\omega^2$). In fact, pulse shaping is achieved by control of the spatial phase which, due to the separation of spectral components in the Fourier plane, translates into spectral phase control [29]. Our model assumes that the Fourier plane of the pulse shaping system is imaged in the Fourier plane of the SSTF setup by the intervening optics (cylindrical lens, grating pair, and cylindrical lens). Thus, the wavefront modulation in the Fourier plane of the shaper is translated into the Fourier plane of the SSTF setup. Application of Fourier optics [10,28,29] to the SSTF setup with a wavefront modulation leads to the calculated spatio-spectral and spatio-temporal distributions shown in Fig. 6. The spatio-spectral and spatio-temporal profiles were calculated for phase ramps corresponding to an unshaped pulse advanced by 1.5 ps and delayed by 1.5 ps. The spectral and temporal distributions for an unshaped pulse are centered at $x=0$ coordinate whereas application of the phase ramp shifts the center of the beam down (negative x coordinate) for a positive 1.5ps phase ramp and up (positive x coordinate) for a negative 1.5ps phase ramp. Replacing the spectral phase term with a spatial phase term in the Fourier plane of the SSTF results in correct prediction of the shifting of the beam in transverse direction, as observed in Fig. 5. This is in addition to shifting the spatio-temporal focus by tuning the second order phase β parameter (not shown). The SSTF optical arrangement, in combination with parametric laser pulse shaping, should be useful for discrimination of features transverse to the beam path. Interestingly, this effect is observed for a double pulse structure when an opposite sign phase ramp are superimposed to create the desired temporal profile. Thus, the simulation results qualitatively agree with all aspects of the experimental data including the pulse front tilt.

In addition to the transverse shift, both pulses shown in Fig. 5 a-e experience the influence of compression up to the temporal focus in a manner similar to the single pulse experiment presented in Fig. 3. Both pulses have a temporal duration of approximately 300 fs at a position 1 mm before the focus, they both compress to a duration of 100 fs at the focus

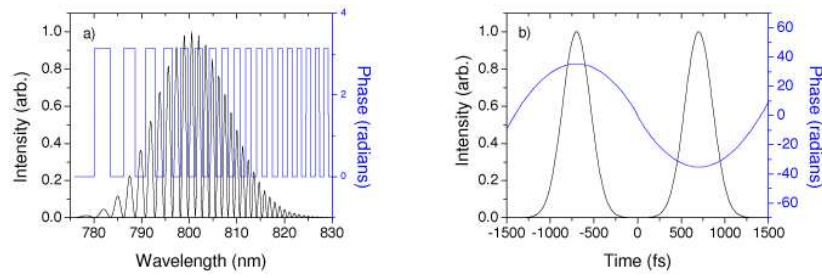


Fig. 7. Theoretical a) spectral phase and intensity and b) temporal phase ($\pm 7000\text{fs}^2$) and temporal intensity shape.

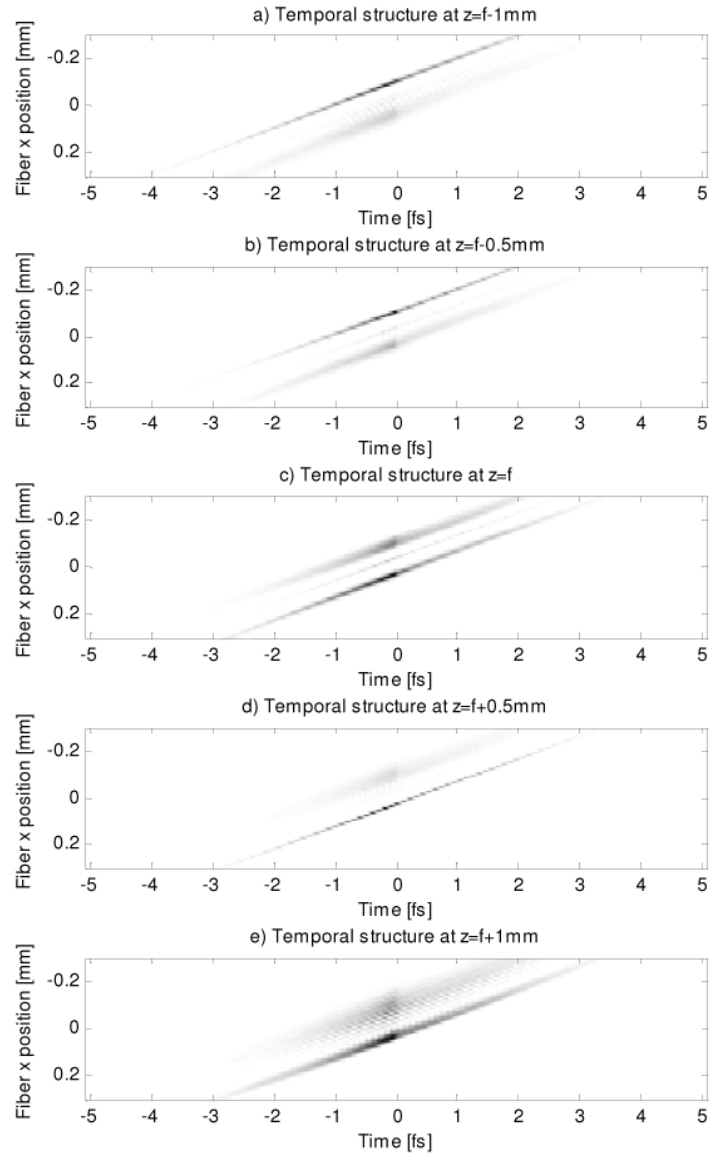


Fig. 8. Measured evolution of the temporal intensity of the two pulse structure from Fig. 6. shaping. a) $z=f-1\text{mm}$ b) $z=f-0.5\text{mm}$ c) $z=f$ d) $z=f+0.5\text{mm}$ e) $z=f+1\text{mm}$, where f is a focal length.

and then disperse to a duration of 1 ps, 1 mm after the focus. The small ghost pulse observed at time zero in Fig. 5 a-e could result from incomplete modulation of the phase and transmission in the pulse shaper and transmission through interpixel gaps. In panels a and e of Fig. 5, the center ghost pulse interferes with the two main pulse fronts, resulting in interference along the pulse fronts.

Figure 5 also shows some asymmetry in the temporal pulse compression and stretching. The asymmetry is due to slight mis-alignment between the position of the temporal focus and the position of the measurements. The temporal focus was determined by locating the most intense portion of the focus with CCD camera in the SEA TADPOLE while scanning the z translation stage. This method determines the position of the spatial focus and since the pulse that enters the SSTF setup contains some GVD, the spatial and temporal foci do not precisely overlap, causing the asymmetry in the temporal compression and stretching of the pulse around $z=0$.

Recent experiments have shown [6] that achieving a high degree of depth resolution in microscopy experiments enhances the investigation of biological samples. Multiple foci have been shown to improve such imaging capabilities [1,30]. We next demonstrate that multiple longitudinal foci can be generated in the SSTF apparatus by combining parametric pulse shaping with SSTF through independent manipulation of the second order phase in each pulse comprising the pulse train. To demonstrate dual longitudinal temporal foci in a single laser beam, we designed two pulses with second order spectral phases of equal magnitude but opposite sign. Each pulse, with a different second order phase profile, compresses at a different spatial coordinate, and thus two spatio-temporal foci are produced at different longitudinal positions. The theoretical pulse shape designed for dual foci is illustrated in Fig. 7. This particular pulse shape was chosen to create the same temporal separation as in Fig. 5 (1.4ps), with the addition of quadratic phases with opposite signs. The resulting evolution of the spatio-temporal profile was measured using SEA TADPOLE is shown in Fig. 8. The measurement demonstrates that the different phases applied to each sub-pulse results in temporal compression at specific longitudinal positions during propagation through the focus. In Fig. 8a, the pulse to the left (centered at $x = -0.1$ mm at 0 fs) is compressed and subsequently stretches in the remaining panels. The pulse to the right (centered at $x = 0.0$ mm at 0fs) compresses to the shortest duration in panel c and then stretches. The longitudinal distance between the pulses can then be controlled by changing the second order phase.

We next consider the formation of three foci from one beam. Such a pulse might be useful for spatio-temporal sensing. To accomplish this, we construct three sub-pulses having negative, zero, and positive second order quadratic temporal phase, respectively. The parametrically designed pulse is illustrated in Fig. 9. The calculated spectral amplitude and phase to produce the necessary temporal features is shown in Fig. 9a. The temporal domain picture reveals that there are three pulses, as illustrated in Fig. 9b. The delay sequence is -700 fs, 0 fs, and 700 fs. The pulses at -700 and 700 fs are specified in the parametric program with positive and negative second order phases. The spatio-temporal characterization of the triple foci experiment using SEA TADPOLE is shown in Fig. 10.

Figure 10a reveals that the duration of pulse 1 is compressed to approximately 100fs while the second and third pulses have much longer duration. Furthermore, the temporal focus for pulse 1 occurs at the shortest longitudinal position in the geometric focus. In Fig. 10b, pulse 2 has the shortest duration, while pulse 1 is temporally stretching and pulse 3 is in the process of temporal compression, but is not fully compressed. Panel d in Fig. 10 shows that pulse 3 is temporally compressed while pulses 1 and 2 are temporally expanding. The last panel shows that all pulses have moved passed their respective spatial temporal foci, all pulse fronts have increased FWHM from their shortest value from preceding panels. In addition to the three pulses focusing at different spatial positions along the axis of propagation (z axis of

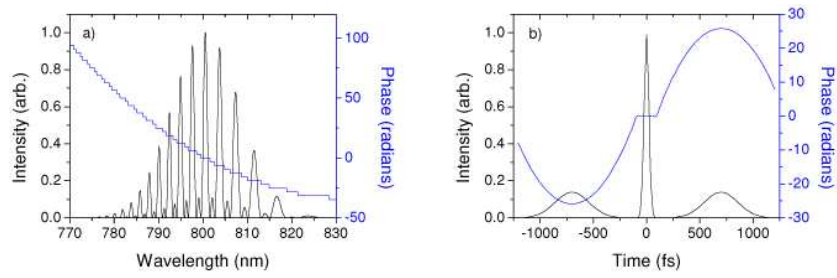


Fig. 9. a) Theoretical spectral phase, intensity and b) temporal phase and intensities. The pulses at (+/-) 700fs have an applied second order chirp of (+/- 7000fs²) and the pulse at 0fs has no applied chirp.



Fig. 10. Measured evolution of the temporal intensity of the two pulse structure from Fig. 9. shaping. a) $z=f-1\text{mm}$ b) $z=f-0.5\text{mm}$ c) $z=f$ d) $z=f+0.5\text{mm}$ e) $z=f+1\text{mm}$, where f is a focal length.

Fig. 2), the linear phase applied to delay the pulses in time also separates the pulse fronts along the transverse, x axis. Once again, the longitudinal distance between the pulses can be increased or decreased by manipulating the second order phase.

Interference effects are observed in Figs. 10a, d, and e wherever the pulse fronts temporally overlap. The user-defined temporal phases of the individual sub pulses lead to defined spatio-temporal interference patterns, with regions of constructive and destructive interference.

The extent to which spatio-temporal control can shift the longitudinal or transverse position of a foci depends on the ability to produce steep phase functions. The difference between two neighboring pixels should not exceed value at which phase wrapping occurs (in our case 4π) due to pixelization. Therefore, there is a maximum lateral and consequently a longitudinal separation that can be achieved with this setup, as quadratic phase profiles will be limited by the same reasons.

Another limitation of this technique is the focal spot resolution. Traditional confocal microscopy has the advantage of spatial resolution in the lateral direction of the focusing beam, as the tighter foci produce spot sizes typically around 20-100nm. With SSTF longitudinal resolution will be orders of magnitude larger because lateral resolution is lost in the wide field technique due to the spatially and spectrally dispersed. However, SSTF benefits in the longitudinal dimension as the temporal compression leads to a thin circular slice through the sample in this dimension.

A spatio-temporal pulse shape which generates 2-3 SSTF foci will permit imaging at different focal planes along the longitudinal focal coordinate. In addition images from laterally displaced focal planes can be obtained with the use of linear phase ramps. The image would be acquired without the use of moving parts, which may enhance the resolution offered by SSTF by reducing the mechanical noise. Multiple foci will also simultaneously produce images from different longitudinal and lateral focal planes.

Our technique offers two dimensional scanning capabilities by combining a one dimensional liquid crystal array standard pulse shaping with and SSTF optics. The scanning domain could be easily extended to three dimensions using a two dimensional liquid crystal modulator in our pulse shaper. This setup would be comparable to the three dimensional scanning offered by a series of acousto-optic deflectors [6] with the additional benefit of spatio-temporal focusing for multiphoton microscopy.

4. Conclusion

These experiments, based on the of the initial studies by Durst et al. [10–12], demonstrate that complex spectral phase and amplitude profiles yields control over the number of foci and the respective transverse and longitudinal positions. The spatio-temporal focusing of a femtosecond pulse has been completely characterized using scanning spectral interferometry. Multiple foci were produced in the transverse and longitudinal directions with respect to the propagation of a single laser beam. The absolute positions of the foci can be controlled using parametric pulse shaping. Multiple temporal foci produced through parametric pulse shaping provide longitudinal and transverse scanning capabilities without the need for mechanical motion.

Acknowledgements

This work was supported by grants from the National Science Foundation CHE No. 331390111 and the Army Research Office No. 311390121.